Los Alamos NATIONAL LABORATORY EST.1943

LA-UR-20-23550 (Accepted Manuscript)

A framework for quantitative analysis of spectral data in two channels

Ryan, Duncan Patrick
Dunlap, Megan Kathryn
Majumder, Somak
Hollingsworth, Jennifer Ann
Werner, James Henry
Van Orden, Alan K
Gelfand, Martin P.
Goodwin, Peter Marvin

Provided by the author(s) and the Los Alamos National Laboratory (2020-09-28).

To be published in: Applied Physics Letters

DOI to publisher's version: 10.1063/5.0013998

Permalink to record: http://permalink.lanl.gov/object/view?what=info:lanl-repo/lareport/LA-UR-20-23550

Disclaimer:
Los Alamos National Laboratory, an affirmative action/equal opportunity employer, is operated by Triad National Security, LLC for the National Nuclear Security Administration of U.S. Department of Energy under contract 89233218CNA000001. By approving this article, the publisher recognizes that the U.S. Government retains nonexclusive, royalty-free license to publish or reproduce the published form of this contribution, or to allow others to do so, for U.S. Government purposes. Los Alamos National Laboratory requests that the publisher identify this article as work performed under the auspices of the U.S. Department of Energy. Los Alamos National Laboratory strongly supports academic freedom and a researcher's right to publish; as an institution, however, the Laboratory does not endorse the viewpoint of a publication or guarantee its technical correctness.

RESEARCH LIBRARY

Applied Physics Letters ACCEPTED MANUSCRIPT
This is the author's peer reviewed, accepted manuscript. However, the online version of record will be different from this version once it has been copyedited and typeset.
PLEASE CITE THIS ARTICLE AS DOI: 10.1063/5.0013998
AIP Publishing

A Framework for Quantitative Analysis of Spectral Data in Two Channels

Duncan P. Ryan,[1] Megan K. Dunlap,[2] Somak Majumder,[1] James H. Werner,[1] Jennifer A. Hollingsworth,[1] Martin P. Gelfand,[3] Alan Van Orden,[2] and Peter M. Goodwin[1, a)]
[1)] *Center for Integrated Nanotechnologies, Los Alamos National Laboratory, Los Alamos, NM, 87545, USA*
[2)] *Department of Chemistry, Colorado State University, Fort Collins, CO, 80523, USA*
[3)] *Department of Physics, Colorado State University, Fort Collins, CO, 80523, USA*

(Dated: 30 June 2020)

The simultaneous acquisition of emission intensity from two channels in dual-color fluorescence measurements can be used to determine the spectral properties of an emitter. We detail a method to extract quantitative information from dual-color measurements by considering two models: a single spectral component model for peak wavelength determination, and a dual spectral component model for relative strength determination. The former model is useful for spectral characterization and establishing heterogeneity within an emitter species while the latter model is useful for analyzing energy transfer efficiency. Both models are formalized to yield probability distributions that reflect uncertainties due to shot-noise. We applied these analysis tools to single-particle measurements of CdSe/CdS quantum dots. Isolated emitters had narrow spectral-intensity distributions that reflected their static emission profiles and fluorescence stability. Small assemblies of mixed donor/acceptor particles exhibited dynamic behavior where emission configuration changes reveal different spectral characteristics due to energy transfer.

The spectral signature of a fluorescent probe can reveal information about its internal electronic configuration or reflect interactions of the probe with its environment. In single-particle experiments, monitoring changes to a spectral profile can show underlying dynamics of a system. For example, energy transfer or fluorescence quenching measurements examine intensity fluctuations among different spectral components to determine the physical state of molecular pairs. With a rigorous interaction model, such experiments can estimate kinetic rates of various recombination pathways and energy transfer for the system, or estimate molecular separation distances with nanometer resolution[1].

Collecting spectral information from an emitter involves placing dispersive optics in the detection path of an instrument. While hyperspectral imaging methods using prisms[2–4] or gratings[5] to generate the complete spectra of emitters have been demonstrated, these approaches require many photons to resolve what are generally simple and predictable spectral profiles. Similarly, engineered point spread functions for spectral imaging[6,7] reduce signal-to-noise by spreading spectral information across a large number of detector elements. Confocal microscopy and dual-view wide-field microscopy for energy transfer measurements typically divide the fluorescence into two color channels with a dichroic beamsplitter[8]. In these approaches, the difference of fractional intensities in each channel, the anisotropy value, quantifies the distribution of the spectral profile into the discrete spectral bins. The anisotropy value is dimensionless and requires a supporting model to extract physical properties such as wavelength or absolute quenching efficiency[9,10].

a)pmg@lanl.gov

We present a general method for analyzing dual-color fluorescence measurements to obtain spectral properties from single-particle experiments. Two models are developed: one to determine the peak wavelength of individual emitters, and one to investigate mixed-species spectral profiles for energy transfer or quenching applications. Both models incorporate instrument spectral response functions (e.g. from beamsplitters and bandpass filters) to improve spectral registration, and are applicable to camera, intensity-based (e.g. photomultiplier tube), and photon counting microscopies. Results from CdSe/CdS quantum dots (QDs) as isolated particles and as interacting systems are presented as demonstrations of the method. This approach offers quantitative spectral interpretation of two color channel data and incorporates shot-noise statistics to provide uncertainty analysis.

The following sections derive the models for calculating either the peak wavelength of an emitter (λ_0) using a single spectral feature or the relative contributions of two emitters (r). In both, the anisotropy value η is determined from experimental data, which may come from binned counts for photon counting measurements or from photon intensity fitting results for image-based experiments. Figure 1(a) illustrates the two models.

The spectral profile arriving at a detector i in a dual-color configuration has the form

$$S_i(\lambda) = g(\lambda|\lambda_0, \sigma) \times f_i(\lambda) \tag{1}$$

where $g(\lambda|\lambda_0, \sigma)$ is a normal distribution representing the spectral profile of the emitter (peak emission at λ_0 with bandwidth σ) and $f_i(\lambda)$ is the spectral response function of all the optics along the path to the detector (dichroic and bandpass filters). The spectral profile of one detection channel is integrated over wavelength and subtracted from that of the other detector channel to

ACCEPTED MANUSCRIPT
Applied Physics Letters
This is the author's peer reviewed, accepted manuscript. However, the online version of record will be different from this version once it has been copyedited and typeset.
PLEASE CITE THIS ARTICLE AS DOI: 10.1063/5.0013998
AIP Publishing

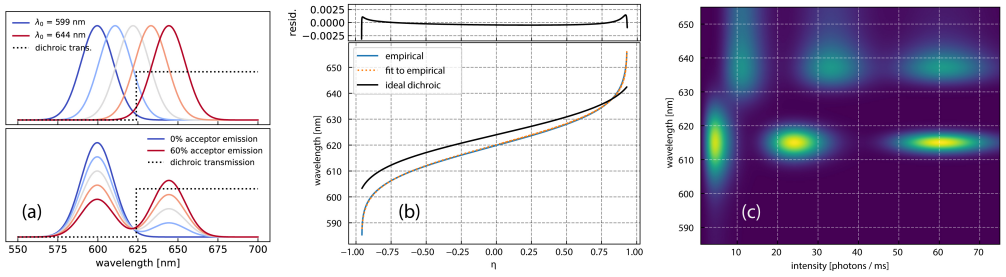

FIG. 1. **(a)** The wavelength model (top) considers how the intensity from a single spectral feature is distributed into two channels by a dichroic mirror when the peak wavelength of the feature is unknown. The ratio model (bottom) considers the intensity distribution from two fixed wavelength sources and determines the relative strength of each component. **(b)** The general form of Eqn. (4) (orange) approximates the empirical calculation (blue) using real spectral response functions $f_i(\lambda)$ well. For reference, the ideal dichroic calibration model from Eqn. (3) is shown (black) to illustrate the impact of ignoring the real spectral response function of the imaging system. **(c)** The spectral-intensity distribution functions for emission at two wavelengths, 615 nm (bottom series) and 637 nm (top series), at three different intensity levels. Each intensity series corresponds to the same η value, but the spectral-distribution functions illustrate how the uncertainty of the wavelength parameter and total intensity are dependent on the individual measurements x_1 and x_2 through Eqn. (8).

obtain the anisotropy value

$$\frac{I_{\text{trans}} - I_{\text{refl}}}{I_{\text{trans}} + I_{\text{refl}}} \equiv \eta = \int S_{\text{trans}}(\lambda)\mathrm{d}\lambda - \int S_{\text{refl}}(\lambda)\mathrm{d}\lambda. \quad (2)$$

With an ideal dichroic beamsplitter and no bandpass filters, $f_i(\lambda)$ can be represented by a step function (or its compliment) at the cutoff wavelength λ_C of the dichroic. In this case, the integrals are straightforward and one obtains the anisotropy value

$$\eta = -\text{erf}\left(\frac{\lambda_C - \lambda_0}{\sqrt{2}\sigma}\right).$$

Solving for the peak emission wavelength λ_0, we obtain

$$\lambda_0(\eta) = \lambda_C + \sqrt{2}\sigma \times \text{erf}^{-1}(\eta). \quad (3)$$

In principle, using Eqn. (3) and the intensities of the transmitted and reflected optical paths to calculate η, the peak emission wavelength could be determined.

However, real spectral response functions $f_i(\lambda)$ do not lead to convenient forms for η that can be inverted to obtain a closed-form solution of λ_0. Motivated by the result of Eqn. (3), we assume that λ_0 can be approximated by the more general form

$$\lambda_0(\eta) = a + b \times \text{erf}^{-1}(c \times \eta + d) \quad (4)$$

where $\{a, b, c, d\}$ are parameters that characterize the set of optical elements (dichroic and filters) used for dual-color measurements. Briefly, trial emission profiles are generated (see Fig. 1(a), top) and Eqn. (1) are numerically integrated for various values of λ_0, generating a table of η values as a function of λ_0. The parameters of the general form of Eqn. (4) are then fit according to the table of (λ_0, η) values. This functional form proves to be a good approximation for the calibration involving real spectral response functions $f_i(\lambda)$, as shown in Fig. 1(b). Alternatively, non-Gaussian spectral profiles (e.g. fluorescent dyes) can be accommodated using this procedure where the parameters conform Eqn. (4) to a calibration curve that reflects the specific spectral profiles. In general, the shape of the spectral profile of the emitter has a lesser impact on the calibration curve than the spectral response functions of the optical elements.

A single peak wavelength is not a good descriptor for a mixed species emission spectrum. For mixed species emission profiles, we must refer to the relative strengths of the emission features. In this case, the peak wavelengths of the two spectral features are fixed (see Fig. 1(a), bottom) and the spectral profile arriving at a detector i is

$$S_i(\lambda) = [(1-r) \times g_{\text{D}}(\lambda) + r \times g_{\text{A}}(\lambda)] \times f_i(\lambda)$$

where r is the relative strength of one emitter to the other (i.e. donor and acceptor particles), $g_i(\lambda) = g(\lambda|\lambda_i, \sigma_i)$, and λ_j, σ_j specify the fixed peak wavelength and linewidth of each species' emission profile, respectively.

Solving Eqn. (2) for the relative strength, we obtain

$$r = \frac{\eta - \int g_{\text{D}}(\lambda) \times [f_{\text{trans}}(\lambda) - f_{\text{refl}}(\lambda)]\,\mathrm{d}\lambda}{\int (g_{\text{A}}(\lambda) - g_{\text{D}}(\lambda)) \times [f_{\text{trans}}(\lambda) - f_{\text{refl}}(\lambda)]\,\mathrm{d}\lambda} = \frac{\eta - C_1}{C_2}. \quad (5)$$

Applied Physics Letters ACCEPTED MANUSCRIPT
This is the author's peer reviewed, accepted manuscript. However, the online version of record will be different from this version once it has been copyedited and typeset.
PLEASE CITE THIS ARTICLE AS DOI: 10.1063/5.0013998
AIP Publishing

In Eqn. (5), the integrals do not depend on any free variables and can be computed directly. Note that this ratio model is linear with respect to η, while the wavelength model derived in the previous section is only approximately linear in the center of the range of η and is strongly non-linear at the extrema of η. This behavior of the wavelength model results in greater uncertainty for peak wavelength values near the extrema, which occurs when emission is weak in one of the two channels.

Equations (4) and (5) allow us to determine either the peak emission wavelength λ_0 (single species measurements) or the relative strength of the longer wavelength emitter r (mixed species measurements) from the transmitted and reflected optical path intensities of a dual-color imaging configuration. Higher photon count rates more precisely determine a λ_0 or r parameter than lower count rates. We incorporate the relevant uncertainties in the form of spectral-intensity distributions.

Spectral-intensity distribution functions are derived by recognizing that the count rates used to determine η, $I_{\text{trans}} = X_1$ and $I_{\text{refl}} = X_2$, are random variables drawn from the joint probability function

$$f_{X_1,X_2}(x_1, x_2|\overline{x}_1, \overline{x}_2) = \text{Pois}(x_1|\overline{x}_1) \times \text{Pois}(x_2|\overline{x}_2).$$

Here, we use Poisson distributions with rate parameters $\overline{x}_i$. Alternatively, gamma distributions can be substituted if it is desirable to use continuous probability functions, i.e. for non-integer photon estimates from intensity fitting as opposed to photon counting, or other distributions that properly represent the noise behavior of the emitter[11,12]. Bivariant transformations of this joint distribution generate the spectral-intensity distributions for each model.

For the wavelength model, the following transformation variables are used

$$Y_1 = \lambda_0 = a + b \times \text{erf}^{-1}\left(c\frac{X_1 - X_2}{X_1 + X_2} + d\right) \tag{6a}$$

$$Y_2 = I_{\text{total}} = X_1 + X_2 \tag{6b}$$

$$X_1 = \frac{Y_2}{2}\left[1 + \frac{1}{c}\text{erf}\left(\frac{Y_1 - a}{b}\right) - \frac{d}{c}\right] \tag{6c}$$

$$X_2 = \frac{Y_2}{2}\left[1 - \frac{1}{c}\text{erf}\left(\frac{Y_1 - a}{b}\right) + \frac{d}{c}\right]. \tag{6d}$$

Similarly, for the ratio model, the following transformation variables are used

$$Y_1 = \eta = \frac{1}{C_2}\left(\frac{X_1 - X_2}{X_1 + X_2}\right) + \frac{C_1}{C_2} \tag{7a}$$

$$Y_2 = I_{\text{total}} = X_1 + X_2 \tag{7b}$$

$$X_1 = \frac{Y_2}{2}(1 + Y_1C_2 - C_1) \tag{7c}$$

$$X_2 = \frac{Y_2}{2}(1 - Y_1C_2 + C_1). \tag{7d}$$

The spectral-intensity distribution functions are thus

$$f_{Y_1,Y_2}(y_1, y_2|\overline{y}_1, \overline{y}_2) = |J(y_1, y_2)| \times f_{X_1,X_2}(x_1, x_2|\overline{x}_1(\overline{y}_1, \overline{y}_2), \overline{x}_2(\overline{y}_1, \overline{y}_2)) \tag{8}$$

where $|J(y_1, y_2)|$ is the absolute value of the Jacobian

$$J(y_1, y_2) = \frac{\partial(x_1, x_2)}{\partial(y_1, y_2)}.$$

The spectral-intensity distribution for detector intensities x_1 and x_2 is calculated by evaluating the distribution function Eqn. (8) across a 2D grid of values $(\overline{y}_2, \overline{y}_1)$. Thus, a spectral-intensity distribution is a 2D likelihood map that the measurement corresponds to an intensity of $\overline{y}_2$ from a spectral parameter (λ_0 or r) of $\overline{y}_1$.

Figure 1(c) illustrates how the spectral-intensity distribution function captures the intrinsic shot-noise uncertainty for the wavelength model. Lower emission rates have greater wavelength uncertainty because an increase or decrease of the number of counts in one detector due to random sampling of a Poisson distribution more significantly impacts the subsequent η value than at higher count rates. Figure 1(c) also demonstrates how the uncertainty is a function of the peak wavelength: distributions are broader near the wavelength extrema than near the middle of the η value range.

We used the wavelength and ratio models to study energy transfer between CdSe/CdS quantum dots (QDs) with a dual-view wide-field microscope. Spectrofluorometry characterization of the donor and acceptor species determined ensemble peak wavelengths of 597 nm and 635 nm, respectively. Energy transferring assemblies[13–15] of mixed emitter species were formed similar to Ryan *et al.*[14] See supplementary material for details about QD synthesis, sample preparation, and microscope setup.

Isolated, individual QDs of both donor and acceptor species were analyzed using the wavelength model. The natural single-particle linewidths reported by Chen *et al.*[16], 10.2 nm, were used as the bandwidth parameter σ for the model spectral profiles. Figure 2(a) shows the spectral-intensity distributions for a representative donor (bottom feature) and acceptor (top feature). Each feature is the average of multiple individual distributions from the frames of an image series. Thus, the likelihood maps combine many individual measurements of dual-color intensity pairs.

As Fig. 2(a) shows, the spectral-intensity signatures of individual QDs were narrowly distributed and well determined (although the widths of the spectral profiles, parameters of the model, are broader than the uncertainties and do overlap). These QDs also had stable fluorescence intensities, represented by the narrow distributions along the intensity axis. The comet tails in both distributions illustrate how confined the emissions were to either the short or long wavelength detection channels: these QDs had anisotropy values in the region of the calibration curves where the wavelength uncertainties were large. The spectral-intensity distributions also demonstrate how well the donor and acceptor species were distinguishable owing to their spectral overlap and the dual-color dichroic/filter selection. Furthermore, there was no correlation between a QD's intensity and its wavelength for the QDs in this study.

Applied Physics Letters ACCEPTED MANUSCRIPT
This is the author's peer reviewed, accepted manuscript. However, the online version of record will be different from this version once it has been copyedited and typeset.
PLEASE CITE THIS ARTICLE AS DOI: 10.1063/5.0013998
AIP Publishing

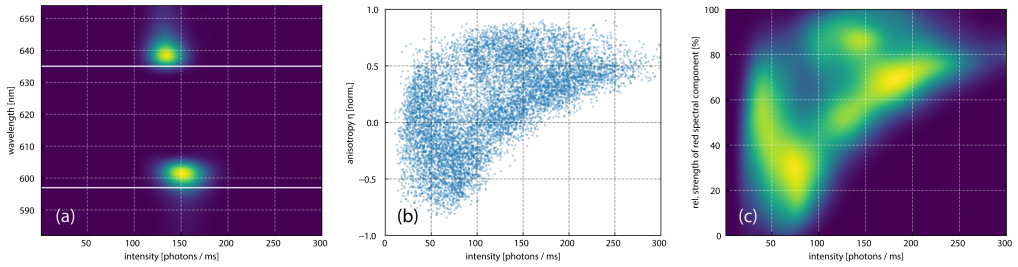

FIG. 2. Application of wavelength and ratio models to QDs and QD clusters. **(a)** The spectral-intensity distributions of an acceptor QD (upper feature) and a donor QD (lower feature). Each QD was imaged separately. Solid horizontal lines indicate the median wavelength from ensemble spectrofluorimetry measurements of each QD species. **(b)** Raw measurements of η and total intensity from an interacting QD cluster. Each point represents the relative channel intensity for a single 50 ms frame of the entire measurement. **(c)** The ratio-intensity distribution for the same QD cluster. The ratio-intensity distribution was calculated for each point in (b) and combined to form the composite distribution. In addition to contributing a meaningful scale for interpreting the cluster dynamics, this representation highlights different emission configuration states the cluster transitioned among during the measurement.

Donor/acceptor assemblies exhibited dramatically different spectral behavior. Figure 2(c) shows the spectral-intensity distribution of a QD assembly using the ratio model. Note that in the ratio model the ordinate scale is the relative strength of the red spectral feature (acceptor) and could be used to determine quenching efficiency in some systems. This ratio-intensity distribution is the result of applying the ratio model to thousands of individual frame-pairs from an image series, generating a composite distribution that represents the various emission configurations that were realized and observed during the measurement. Fluorescence intermittancy (blinking) of the constituent QDs in the cluster had the effect of modulating the intensities and changing the spectral signatures, revealing various emission configurations (e.g. acceptor emitting while donor is dark, acceptor dark while donor is emitting, or all QDs emitting). Therefore, the ratio-intensity distribution in Fig. 2(c) depicts the uncertainties associated with each emission configuration.

The ratio-intensity distribution allows interpretation of the fluorescence dynamics. The assembly depicted in Fig. 2(c) produced lower emission intensities in the donor region of the spectrum, which is attributed to quenched emission rates among the donor species as fluorescence decay competes with energy transfer. Emission composed of ∼80 % of the acceptor component correlates with the highest intensity from the assembly. This feature is another manifestation of energy transfer whereby acceptor emission is enhanced by the donor deficit. Finally, the feature at ∼90 % acceptor emission likely is due to a configuration state with only a single acceptor emitting and thus produces a moderate intensity.

Compared to the common correlation scatter plots of anisotropy versus intensity, Fig. 2(b), spectral-intensity distributions are more informative representation of dual-color measurements. The latter presents the spectral information on a scale with direct physical meaning and explicitly conveys the uncertainties intrinsic to the raw data.

Analysis of two color channel data can be enhanced in many situations by spectral models. The models presented in this work yield calibrated scales that are related to physical parameters and incorporate uncertainty analysis. While demonstrated with donor/acceptor QD assemblies, this method also has application for experiments involving dyes or fluorescent proteins. In such energy transfer or quenching experiments, this method is well suited for the higher degree of emitter spectral overlap. Furthermore, this approach can be applied to photon counting, intensity discriminating, or camera-based experiments, and does not require that intensity measurements come from diffraction-limited spots (e.g. spatial mapping).

See supplementary material for additional information about QD synthesis and microscope setup. The data that support the findings of this study are available from the corresponding author upon reasonable request.

ACKNOWLEDGMENTS

Research presented in this article was supported by the Laboratory Directed Research and Development program of Los Alamos National Laboratory under project #20180189ER. This work was performed, in part, at the Center for Integrated Nanotechnologies, an Office of Science User Facility operated for the U.S. Department of Energy (DOE) Office of Science by Los Alamos National Laboratory (Contract 89233218CNA000001). LA-UR-20-23550.

Applied Physics Letters ACCEPTED MANUSCRIPT
This is the author's peer reviewed, accepted manuscript. However, the online version of record will be different from this version once it has been copyedited and typeset.
PLEASE CITE THIS ARTICLE AS DOI: 10.1063/5.0013998
AIP Publishing

[1]L. Stryer and R. P. Haugland, Proceedings of the National Academy of Sciences **58**, 719 (1967).
[2]Z. Zhang, S. J. Kenny, M. Hauser, W. Li, and K. Xu, Nature Methods **12**, 935 (2015).
[3]M. J. Mlodzianoski, N. M. Curthoys, M. S. Gunewardene, S. Carter, and S. T. Hess, PLOS ONE **11**, e0147506 (2016).
[4]T. Huang, C. Phelps, J. Wang, L.-J. Lin, A. Bittel, Z. Scott, S. Jacques, S. L. Gibbs, J. W. Gray, and X. Nan, Biophysical Journal **114**, 301 (2018).
[5]B. Dong, L. Almassalha, B. E. Urban, T.-Q. Nguyen, S. Khuon, T.-L. Chew, V. Backman, C. Sun, and H. F. Zhang, Nature Communications **7**, 1 (2016).
[6]Y. Shechtman, L. E. Weiss, A. S. Backer, M. Y. Lee, and W. E. Moerner, Nature Photonics **10**, 590 (2016).
[7]C. Smith, M. Huisman, M. Siemons, D. Grünwald, and S. Stallinga, Optics Express **24**, 4996 (2016).
[8]S. Hohng, C. Joo, and T. Ha, Biophysical Journal **87**, 1328 (2004).
[9]E. A. Jares-Erijman and T. M. Jovin, Nature Biotechnology **21**, 1387 (2003).
[10]J. J. McCann, U. B. Choi, L. Zheng, K. Weninger, and M. E. Bowen, Biophysical Journal **99**, 961 (2010).
[11]C. H. H. Schulte, J. Hansom, A. E. Jones, C. Matthiesen, C. L. Gall, and M. Atatüre, Nature **525**, 222 (2015), number: 7568 Publisher: Nature Publishing Group.
[12]E. B. Flagg, S. V. Polyakov, T. Thomay, and G. S. Solomon, Physical Review Letters **109**, 163601 (2012), publisher: American Physical Society.
[13]D. P. Shepherd, K. J. Whitcomb, K. K. Milligan, P. M. Goodwin, M. P. Gelfand, and A. Van Orden, The Journal of Physical Chemistry C **114**, 14831 (2010).
[14]D. P. Ryan, P. M. Goodwin, C. J. Sheehan, K. J. Whitcomb, M. P. Gelfand, and A. Van Orden, The Journal of Physical Chemistry C **122**, 4046 (2018).
[15]M. K. Dunlap, D. P. Ryan, P. M. Goodwin, J. H. Werner, S. Majumder, J. A. Hollingsworth, M. P. Gelfand, and A. Van Orden, Applied Physics Letters **116**, 021103 (2020).
[16]O. Chen, J. Zhao, V. P. Chauhan, J. Cui, C. Wong, D. K. Harris, H. Wei, H.-S. Han, D. Fukumura, R. K. Jain, and M. G. Bawendi, Nature Materials **12**, 445 (2013).

AIP Publishing

Applied Physics Letters ACCEPTED MANUSCRIPT

This is the author's peer reviewed, accepted manuscript. However, the online version of record will be different from this version once it has been copyedited and typeset.

PLEASE CITE THIS ARTICLE AS DOI: 10.1063/5.0013998

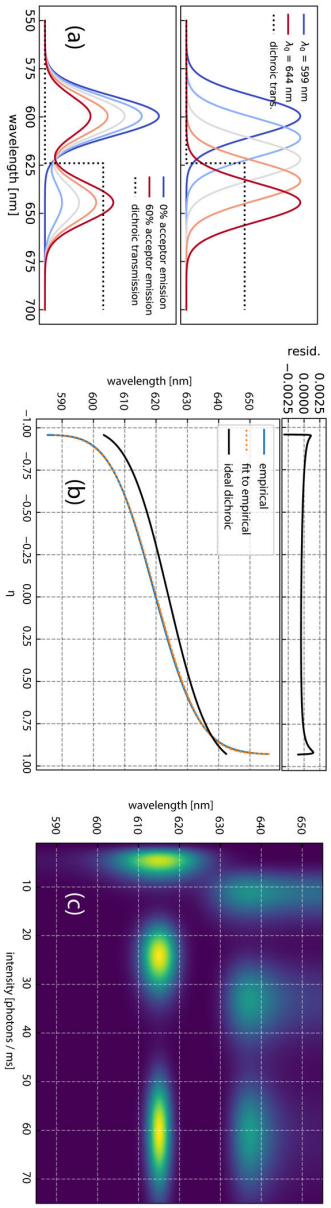

AIP Publishing

Applied Physics Letters ACCEPTED MANUSCRIPT

This is the author's peer reviewed, accepted manuscript. However, the online version of record will be different from this version once it has been copyedited and typeset.
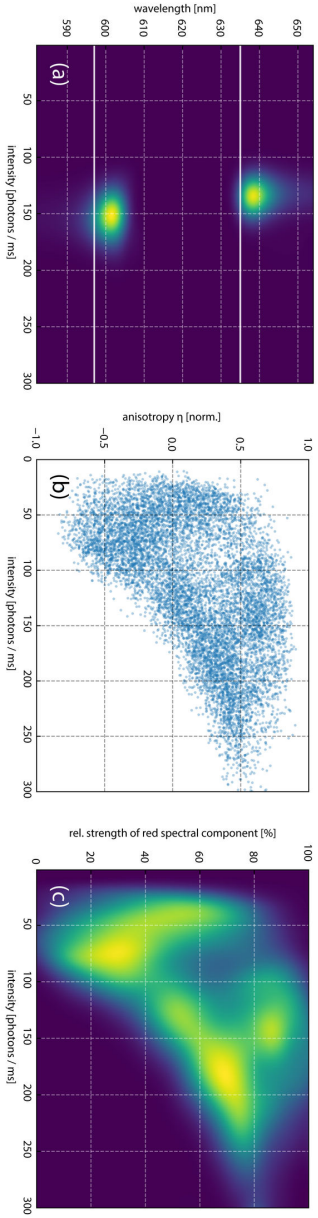
PLEASE CITE THIS ARTICLE AS DOI: 10.1063/5.0013998